

Fig. 3. Diatom biomass in the DCM. **(A)** Diatom biomass versus depth ($\mu\text{g C L}^{-1}$) during the decline of a diatom bloom; $t = 0$ (solid circles) denotes the first sampling of the bloom. Repeated samplings on days 3 and 8 after the initial encounter depicted by solid squares and diamonds, respectively. For comparison, the OUT station is also shown (crosses). **(B)** An epifluorescent image of the phytoplankton population within the DCM at the OUT station. **(C and D)** Epifluorescent images of the phytoplankton population within the DCM at the center of Cyclone Opal during the initial sampling [$t = 0$ day (C)] and 8 days later [$t = 8$ days (D)] during the bloom decline. Images were taken of slides viewed at 200 \times magnification, and each image represents $>8 \mu\text{m}$ cells from 500 ml of preserved seawater (9). The red color reflects chlorophyll autofluorescence. Note the transition in diatom species from large centric genera (*Rhizosolenia* and *Chaetoceros*) to smaller genera (for example, *Mastogloia*).

those density layers from lighted surface waters. Thus, elemental constituents locked into eddies by efficient remineralization are exported but not effectively sequestered on annual time scales, because they reside immediately below the euphotic zone. Nonetheless, if eddies function as selective silica pumps (14), these sub-euphotic waters will be disproportionately depleted in silicic acid. To the extent that Si-limitation modulates diatom growth and biomass accumulation, one long-term consequence of repeated nutrient entrainment by wind-driven eddies may be to reduce diatom response, further complicating explanations of how these features affect open-ocean biogeochemistry.

References and Notes

- R. R. Bidigare *et al.*, *Geophys. Res. Lett.* **30**, 1318 (2003).
- D. J. McGillicuddy *et al.*, *Nature* **394**, 263 (1998).
- A. Oschlies, *Deep-Sea Res. I* **48**, 2173 (2001).
- W. Patzert, "Eddies in Hawaiian Islands report no. HIG-69-8" (University of Hawaii, Honolulu, 1969).
- C. Chavanne, P. Flament, R. Lumpkin, B. Dousset, A. Bentamy, *Can. J. Remote Sensing* **28**, 466 (2002).
- M. P. Seki *et al.*, *Geophys. Res. Lett.* **28**, 1583 (2001).
- R. Vaillancourt, J. Marra, M. Seki, M. Parsons, R. Bidigare, *Deep-Sea Res. I* **50**, 829 (2003).
- P. Falkowski, D. Ziemann, Z. Kolber, P. Bienfang, *Nature* **352**, 55 (1991).
- Materials and methods are available on Science Online.
- K. Coale *et al.*, *Science* **304**, 408 (2004).
- K. Coale *et al.*, *Nature* **383**, 495 (1996).
- R. Scharek, M. Latasa, D. M. Karl, R. R. Bidigare, *Deep-Sea Res. I* **46**, 1051 (1999).
- S. Emerson *et al.*, *Nature* **389**, 951 (1997).
- R. Dugdale, F. Wilkerson, H. Minas, *Deep-Sea Res. I* **42**, 697 (1995).
- S. J. Giovannoni, M. S. Rappé, in *Microbial Ecology of the Oceans*, D. L. Kirchman, Ed. (Wiley-Liss, New York, 2000), p. 47.
- E. F. DeLong, D. G. Franks, A. L. Alldredge, *Limnol. Oceanogr.* **38**, 924 (1993).
- H. Reichenbach, in *The Prokaryotes*, A. Barlows, Ed. (Springer-Verlag, New York, 1992), p. 3631.
- C. R. Benitez-Nelson, K. O. Buesseler, D. M. Karl, J. Andrews, *Deep-Sea Res. I* **48**, 2595 (2001).
- L. W. Juranek, P. D. Quay, *Global Biogeochem. Cycles* **19**, 10.1029/2004GB002384 (2005).
- R. Eppley, B. Peterson, *Nature* **282**, 677 (1979).
- E. A. Laws, P. G. Falkowski, W. O. Smith, H. Ducklow, J. J. McCarthy, *Global Biogeochem. Cycles* **14**, 1231 (2000).
- K. O. Buesseler, *Global Biogeochem. Cycles* **12**, 297 (1998).
- D. Nelson, M. Brzezinski, *Limnol. Oceanogr.* **42**, 473 (1997).
- O. Ragueneau, N. Dittert, P. Pondaven, P. Tréguer, L. Corrin, *Deep-Sea Res. II* **49**, 3127 (2002).
- A. F. Michaels, M. W. Silver, *Deep-Sea Res.* **35**, 473 (1988).
- P. Boyd, P. Newton, *Deep-Sea Res. I* **46**, 63 (1999).
- M. Landry *et al.*, *Mar. Ecol. Prog. Ser.* **201**, 57 (2000).
- C. Sakamoto *et al.*, *J. Geophys. Res.* **109**, 10.1029/2003JC001976 (2004).
- A. Morel, *J. Geophys. Res.* **93**, 10749 (1988).
- Our sincere thanks are due to R. R. Bidigare III and R. Styles for help with sample collection and analyses; D. M. Karl, P. Falkowski, and M. Gorbunov for equipment and allowing their students and postdoctoral fellows to participate; and the captain and crew of the R/V *Wecoma*. This research was supported by the Ocean Sciences Division of the NSF. P.M. was supported by a grant from the Gordon and Betty Moore Foundation.

Supporting Online Material

www.sciencemag.org/cgi/content/full/316/5827/1017/DC1

Materials and Methods

References

12 October 2006; accepted 26 March 2007

10.1126/science.1136221

Eddy/Wind Interactions Stimulate Extraordinary Mid-Ocean Plankton Blooms

Dennis J. McGillicuddy Jr.,^{1*} Laurence A. Anderson,¹ Nicholas R. Bates,² Thomas Bibby,^{3,4} Ken O. Buesseler,¹ Craig A. Carlson,⁵ Cabell S. Davis,¹ Courtney Ewart,⁵ Paul G. Falkowski,³ Sarah A. Goldthwait,^{6,7} Dennis A. Hansell,⁸ William J. Jenkins,¹ Rodney Johnson,² Valery K. Kosnyrev,¹ James R. Ledwell,¹ Qian P. Li,⁸ David A. Siegel,⁵ Deborah K. Steinberg⁶

Episodic eddy-driven upwelling may supply a significant fraction of the nutrients required to sustain primary productivity of the subtropical ocean. New observations in the northwest Atlantic reveal that, although plankton blooms occur in both cyclones and mode-water eddies, the biological responses differ. Mode-water eddies can generate extraordinary diatom biomass and primary production at depth, relative to the time series near Bermuda. These blooms are sustained by eddy/wind interactions, which amplify the eddy-induced upwelling. In contrast, eddy/wind interactions dampen eddy-induced upwelling in cyclones. Carbon export inferred from oxygen anomalies in eddy cores is one to three times as much as annual new production for the region.

Understanding the controls on primary production in the upper ocean is of fundamental importance for two main reasons. First, primary productivity sets a first-order

constraint on the energy available to sustain oceanic ecosystems. Second, fixation and subsequent sinking of organic particles remove carbon from the surface ocean (the so-called biological

pump), which plays a key role in the partitioning of carbon dioxide between the ocean and atmosphere. Geochemical estimates of new production (I) surpass the apparent rate of nutrient supply by vertical mixing by a factor of 2 or more in subtropical oceans (2–6), which constitute some of the largest biomes on Earth. Two possible mechanisms to supply the “missing” nutrients locally include nitrogen fixation by cyanobacteria (7–10) and intermittent upwelling by mesoscale eddies and submesoscale processes (11–21).

¹Woods Hole Oceanographic Institution, Woods Hole, MA 02543–1541, USA. ²Bermuda Institute of Ocean Sciences, Ferry Reach, GE01, Bermuda. ³Institute of Marine and Coastal Sciences, Rutgers University, New Brunswick, NJ 08901–8521, USA. ⁴School of Ocean and Earth Science, National Oceanography Centre, University of Southampton, Southampton SO14 3ZH, UK. ⁵University of California, Santa Barbara, CA 93106, USA. ⁶Virginia Institute of Marine Science, Gloucester Point, VA 23062–1346, USA. ⁷Humboldt State University, Arcata, CA 95521, USA. ⁸Rosenstiel School of Marine and Atmospheric Science, University of Miami, Miami, FL 33149, USA.

*To whom correspondence should be addressed. E-mail: dmccgillcuddy@whoi.edu

There are at least three types of mid-ocean eddies in the northwestern subtropical Atlantic: cyclones, anticyclones, and mode-water eddies (Fig. 1A). Cyclones dome both the seasonal and main pycnoclines, whereas regular anticyclones depress both density interfaces. Mode-water eddies derive their name from the thick lens of water that deepens the main pycnocline while shoaling the seasonal pycnocline. Because the geostrophic velocities are dominated by depression of the main pycnocline, the direction of rotation in mode-water eddies is the same as in regular anticyclones. However, displacement of the seasonal pycnocline is the same as in cyclones: Both types of features tend to upwell nutrients into the euphotic zone during their formation and intensification phases. As these eddies spin down, the density surfaces relax back to their mean positions, and thus decaying cyclones and mode-water eddies will have downwelling in their interiors. This temporal evolution during the life cycle of an eddy is a key regulator of the biogeochemical response (22, 23).

Eddy features are readily discernible via satellite altimetry (Fig. 1B and fig. S1). Access

to these data in near-real time (24) facilitates the tracking of individual eddies and adaptive sampling in shipboard operations. In 2004 and 2005, we sampled a total of 10 different eddies, 5 more than once (table S1). Time series within target features allow the resolution of temporal dynamics in eddy-driven nutrient supply, phytoplankton physiological response, changes in community structure, and biogeochemical fluxes. We focus this discussion on cyclone C1 and mode-water eddy A4; findings in other cyclones and mode-water eddies in this study (table S1) as well as prior investigations (table S2) are consistent with those presented here.

Cyclone C1 was occupied by ships four times between June and August 2004 (25). Shipboard acoustic Doppler current profiler (ADCP) data documented the counterclockwise flow associated with C1's negative sea-level anomaly (SLA), and its altimetric history suggested intensification in May. Uplift of near-surface isopycnals was associated with shoaling and enhancement of the subsurface chlorophyll maximum. The magnitude of the subsurface chlorophyll maximum in C1 was lower than in other cyclones (Fig. 2A), yet still in the upper quartile of all subsurface maxima observed in the Bermuda Atlantic Time-series Study (BATS) (26) from 1988 to 2003.

Phytoplankton species composition in cyclone C1 resembled mean conditions at the BATS site (Fig. 2B). On average, *Prochlorococcus* spp., *Synechococcus* spp., pelagophytes, and prymnesiophytes constitute the largest fractions of total chlorophyll a in the depth interval from 75 to 140 m (deep chlorophyll maximum) at the BATS site; diatoms, dinoflagellates, and prasinophytes contribute comparatively little to total chlorophyll a. The eddy-induced bloom in C1 increased the relative amount of *Prochlorococcus* spp. and decreased the relative amount of *Synechococcus* spp., and the rare groups constituted an even smaller fraction of total chlorophyll a.

In subsequent occupations of cyclone C1, conditions at the eddy center changed from a local maximum to a local minimum in chlorophyll a and fluorescence. During this latter phase, integrated primary production at the eddy center was not statistically distinguishable from climatological summertime conditions at the BATS site, nor were bacterial production and biomass (table S3). However, systematic mesoscale variability was observed in microbial parameters, with biomass and production enhancement at the periphery relative to the eddy center. Zooplankton biomass was also elevated on the periphery relative to the eddy center, with large zooplankton migrators (>5 mm) increasing most. Although zooplankton biomass was not significantly different from the long-term BATS summertime mean (1994–2005), there was significant enhancement [analysis of variance (ANOVA), $P < 0.05$] above mean summertime conditions for 2004–2005 (table S3).

Export measured with drifting sediment traps was below the BATS summertime mean, al-

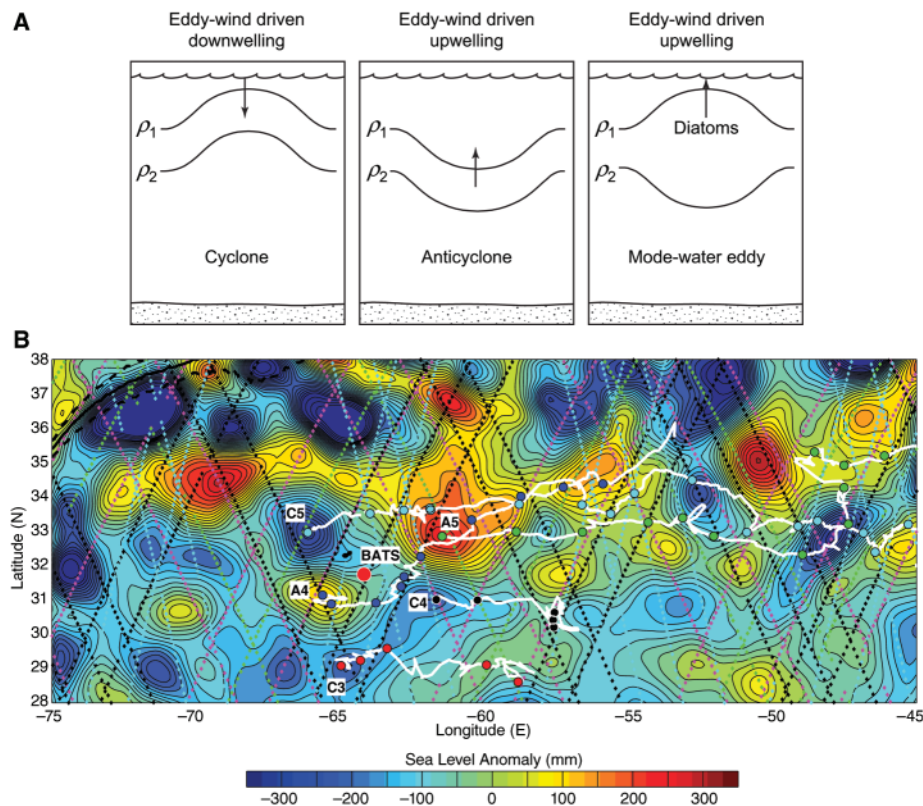


Fig. 1. (A) Isopycnal displacements associated with three types of eddies. Two density surfaces are depicted: one in the seasonal thermocline ρ_1 and one in the main thermocline ρ_2 . Arrows indicate the sense of the vertical velocity arising from the interaction of the wind with the underlying eddy-driven flow, which is upward in anticyclones and mode-water eddies and downward in cyclones. This eddy/wind interaction stimulates diatom blooms in mode-water eddies. (B) Objective analysis of SLA for 17 June 2005, just before the first cruise of the 2005 field season. The Gulf Stream mean path and meander envelope (1 SD) are indicated as solid and dashed black lines, respectively. Prior trajectories of the features of interest are indicated by white lines emanating from eddy centers, with dots at 30-day intervals. Satellite ground tracks are shown for the Jason (magenta), Topex 2 (green), Geosat Follow-on (black), and European Remote Sensing/Envisat (light blue) satellites. A corresponding map for the 2004 field season is provided in fig. S1.

though not anomalously so, given the variability at the BATS site (table S3). ^{234}Th -based export fluxes were consistent with these findings (table S3). However, subsurface oxygen distributions suggest a substantial export event before our observations. During the first occupation, cyclone C1 contained an oxygen minimum in the depth interval from 200 to 400 m (27), in which the oxygen concentrations were lower than all previous measurements at the BATS site in that stratum (Fig. 2C). Nitrate and dissolved inorganic carbon were also enhanced in the feature, in approximately Redfield proportion with the oxygen anomaly. One month later, the magnitude of the oxygen anomaly had decreased by 50% (Fig. 2C). Thus, the oxygen deficit appears to be an ephemeral feature, with a time scale shorter than the lifetime of the eddy.

An estimate of remineralization implied by the oxygen deficit can be computed from differences in oxygen inventories inside versus outside the eddy in this depth interval (Fig. 2C) (28). Using photosynthetic stoichiometry of 138 O_2 :106 C:16 N:1 P, remineralization is 1.4 mol of N m^{-2} , which is approximately three times the annual new production for the region (3). Water mass analysis suggests that the eddy core may have had a distant origin in the southern Sargasso Sea. Using biogeochemical characteristics of the distant waters as the background from which the anomaly is computed, the implied remineralization is 0.7 ± 0.2 mol of N m^{-2} , which is approximately 1.4 times the annual new production at the BATS site.

Mode-water eddy A4 was occupied six times between June and September 2005. Its

SLA was positive (Fig. 1B), and shipboard ADCP measurements confirmed anticyclonic flow. Its altimetric history suggested a relatively persistent SLA of 20 cm for the 4 months preceding our first occupation.

High-resolution surveys with a towed undulating Video Plankton Recorder (29) revealed an extraordinary phytoplankton bloom in the interior of A4 (Fig. 3A). Although submesoscale variability was evident, the enhancement spanned the eddy's inner core (30). Peak chlorophyll a measured near the eddy center was $1.4 \mu\text{g}$ of chlorophyll a liter $^{-1}$, eclipsing the highest value ever measured at the BATS site by a considerable margin (Fig. 2A). This measurement is 8 SD above the mean subsurface maximum at the BATS site.

Phytoplankton species composition in mode-water eddy A4 departed dramatically from mean

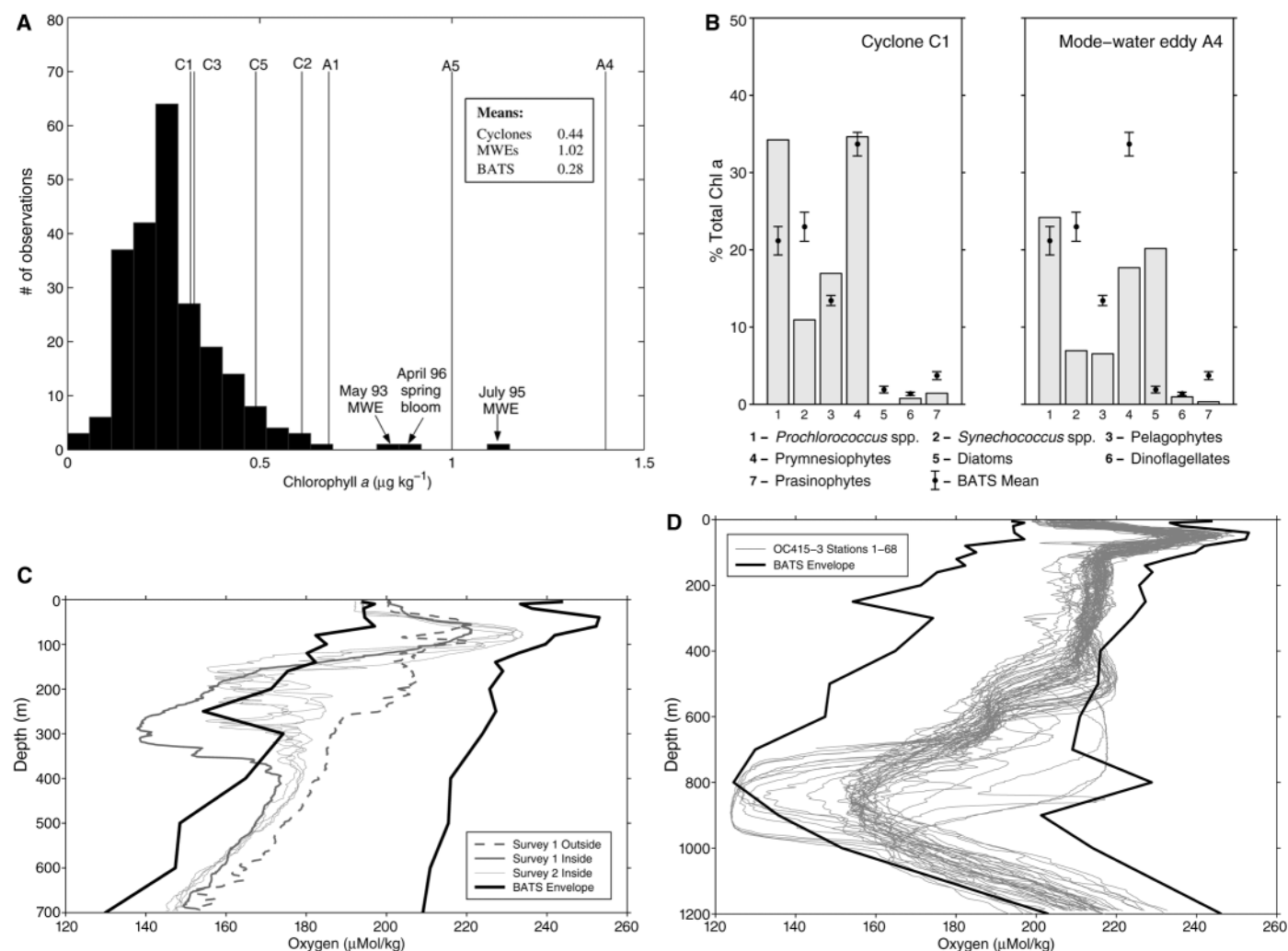


Fig. 2. (A) Histogram of subsurface maxima in chlorophyll a from BATS data from 1998 to 2003. Peak chlorophyll a values in cyclones (C1, C2, C3, and C5) and mode-water eddies (A1, A4, and A5) from the present observations (table S1) are indicated by thin vertical lines. (Inset) Means of the peak chlorophyll a concentrations (micrograms per kilogram) in cyclones and mode-water eddies (MWEs) from the present observations, compared to the mean subsurface maximum from BATS. (B) Phytoplankton species composition (at the depth interval from 75 to 140 m) in cyclone C1 (OC404-1 station 18) and mode-

water eddy A4 (OC415-1 station 16). Estimates of the relative abundance (by pigment mass) of seven different groups, expressed as the percentage of total chlorophyll (Chl) a, were calculated from high-performance liquid chromatography pigment data together with the algorithms described in (53). Means and associated 95% confidence intervals for each group, derived from the BATS data for 1989–2003, are indicated in both plots. (C and D) Oxygen profiles in cyclone C1 (C) and mode-water eddy A4 (D). The envelope of BATS measurements from 1988 to 2003 is indicated by bold lines.

conditions at the BATS site (Fig. 2B), expressed primarily in a shift toward a diatom-dominated community (31). The amount of chlorophyll a

in diatoms in A4 was 8 SD above the BATS mean. Shipboard microscopic cell counts from a sample in the high-chlorophyll region indicated

~8000 colonies liter⁻¹ of the chain-forming diatom *Chaetoceros* spp. Given that each colony contained ~15 cells, we estimate the diatom

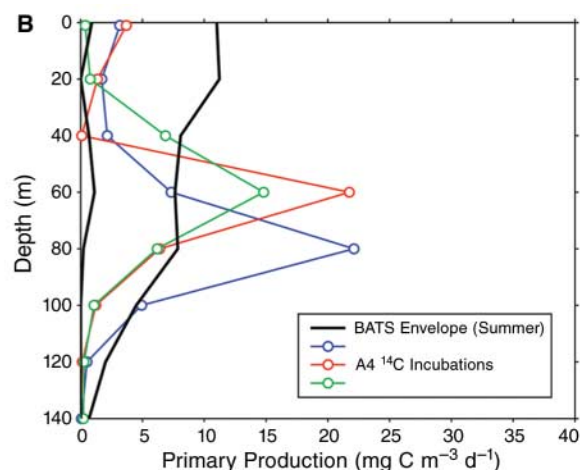
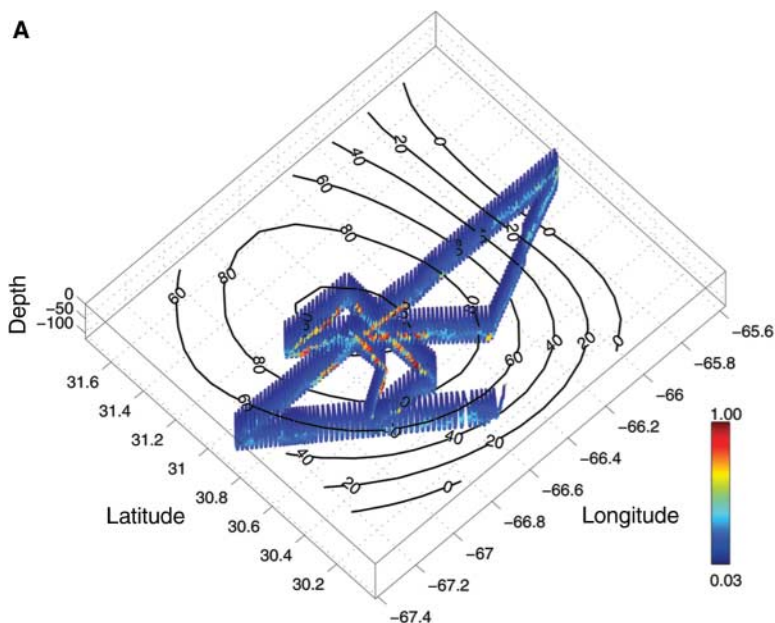
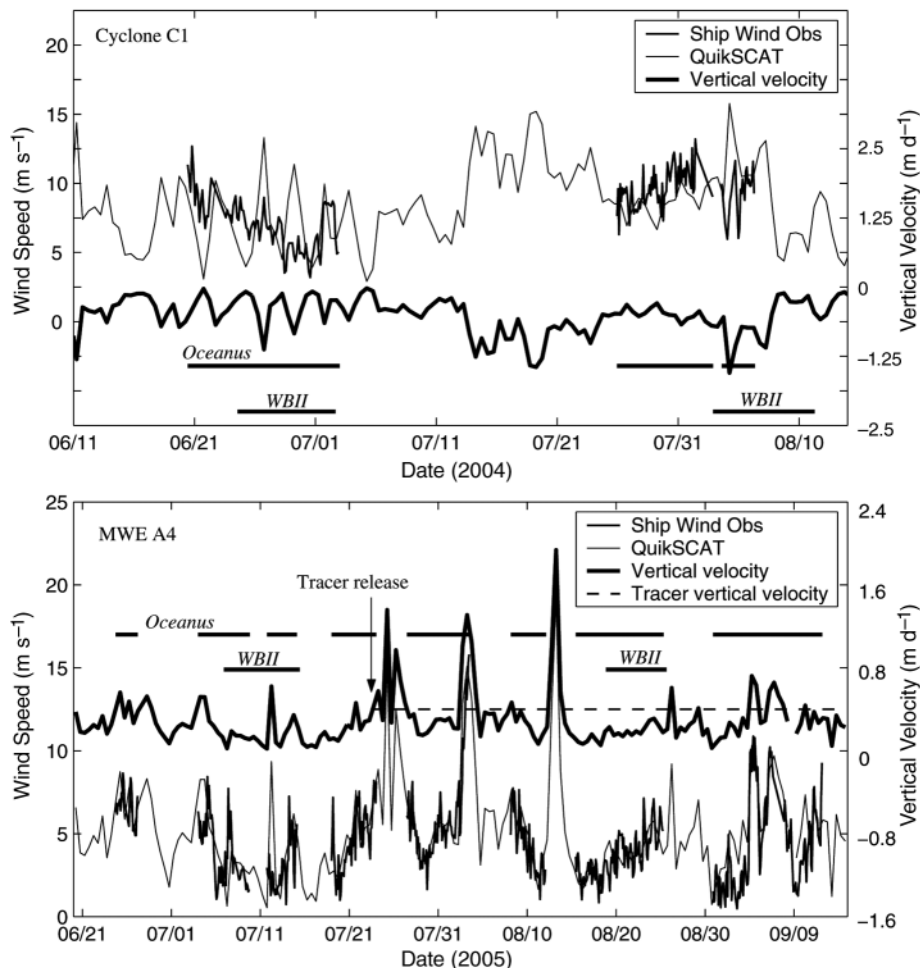


Fig. 3. (A) Three-dimensional distribution of chlorophyll a fluorescence (in relative units) from a Video Plankton Recorder survey of A4, overlaid on contours of SLA (in millimeters) from objectively analyzed satellite data as in Fig. 1B. **(B)** ¹⁴C primary production profiles inside mode-water eddy A4 in August 2005. The minimum and maximum of BATS summertime observations from 1988 to 2003 are indicated by thick black lines.

Fig. 4. Winds and computed vertical velocities arising from wind/eddy interactions in cyclone C1 (**top**) and mode-water eddy A4 (**bottom**). Satellite-based wind measurements along the eddy trajectories (determined by satellite altimetry and shipboard observations) were obtained from QuikSCAT level-3 data, available on a 0.25° twice-daily global grid (see <http://podaac.jpl.nasa.gov/quikscat/>). Time periods of ship occupations by R/V *Oceanus* and R/V *Weatherbird II* (WBII) are indicated by horizontal bars. Shipboard wind observations (R/V *Oceanus*) reveal excellent agreement with the satellite-based measurements. Vertical velocities at the eddy center were computed with the formulas of Martin and Richards (40), assuming a spatially uniform wind over the eddy. The use of a spatially variable wind introduces additional high-frequency fluctuations in vertical velocity, but their impact on the mean is less than 10%. Vertical velocity estimated from a sulfur hexafluoride tracer release in mode-water eddy A4 (0.4 m day⁻¹) for the time period between the release and the final survey is indicated by a dashed line in the lower panel.



concentration to have been four to five orders of magnitude above the background concentration of 1 to 10 cells liter⁻¹. The propensity of mode-water eddies to form diatom blooms emerges as a systematic aspect of these data (table S1) and prior observations (table S2): The three highest chlorophyll *a* values in the present data and two of the three highest values in the BATS time series (22, 32) (Fig. 2A) were all associated with diatom-dominated phytoplankton communities in mode-water eddies (33).

In the first occupation of mode-water eddy A4, primary production was not significantly different from mean summertime conditions at the BATS site. In the second occupation, primary production was significantly enhanced (table S3) (34). The primary production anomaly had an unusual vertical structure, with a subsurface maximum that exceeded the envelope of BATS observations in the depth interval from 60 to 80 m (Fig. 3B). This structure is consistent with enhanced nutrient supply from below and a diatom population capable of high growth rates in low-light conditions (35, 36).

Zooplankton biomass at the eddy center varied more than threefold (table S3). Maximum vertically integrated biomass occurred at the same location as the anomalously high primary production (Fig. 3B), with the largest increase in the 1- to 5-mm size range. Zooplankton biomass in A4 was higher than in 2004–2005 BATS summer samples but not significantly different (ANOVA, $P > 0.05$) from the long-term BATS summer mean (table S3). However, samples from cyclones and mode-water eddies constitute 6 of the top 10 highest zooplankton biomass observations in the combined data set.

Export measured in A4 was below the BATS summertime mean, although within the range of variability observed at the BATS site (table S3). ²³⁴Th-based export flux estimates yielded similar values (table S3). The bloom in A4 was accompanied by exceptionally low oxygen concentrations (~120 μmol kg⁻¹) in the depth interval from 800 to 1000 m (Fig. 2D), which is lower than ever measured at the BATS site. Remineralization implied by the difference between the observed oxygen deficit inside the eddy and background conditions outside the eddy was 0.8 mol of N m⁻² (28), which is ~1.6 times the annual new production for the region. As in cyclone C1, the oxygen deficit coincided with a discernible salinity anomaly, suggesting that the water mass may have had a distant origin. The climatological salinity distribution (37) indicates potential origins along the northern and southern limbs of the subtropical gyre. The latter contains oxygen concentrations comparable to that observed in the core of A4, whereas the former contains much more oxygen. Thus, the southern source region implies that the oxygen deficit is primarily an advective feature, whereas the northern source region requires a substantial eddy-induced export event (38).

Why is the biological response to cyclones and mode-water eddies so different? Macro-

nutrient stoichiometries just below the euphotic zone are similar (39), suggesting a physical cause. We hypothesize that the difference arises from asymmetry in vertical motions induced by eddy/wind interactions. To quantify this effect, we used a model of uniform wind blowing over an idealized anticyclonic vortex, with wind stress formulated as the difference between air and water velocities at the sea surface (40). Stress is enhanced on the flank of the eddy where wind and current oppose each other, and stress is reduced on the flank where they flow in the same direction. This generates a divergence in the center of an anticyclone regardless of wind direction. Applying this model to A4, the upwelling velocity induced by the eddy/wind interaction ranges from 0.1 to 1.6 m day⁻¹ (Fig. 4) (41). Upward motion in the interior of A4 was confirmed by a tracer release experiment, during which the tracer moved upward at 0.4 m day⁻¹, almost exactly the rate predicted from the eddy/wind interaction model (Fig. 4).

The eddy/wind interaction model predicts downwelling in the interior of cyclone C1 (Fig. 4). The low biomass and productivity at the eddy center during the latter stages of our observations are consistent with the predicted eddy/wind-induced downwelling. Unfortunately, there was no tracer release in C1 that can be used to test this prediction. Nevertheless, it is clear that eddy/wind interactions enhance the vertical nutrient flux in mode-water eddies, and they counterbalance it in cyclones (Fig. 1A). This may explain why phytoplankton enhancement in cyclones is rather ephemeral, whereas mode-water eddies can produce long-lasting blooms of diatoms (42).

Observations presented here document eddy-driven events that exceeded the envelope of variability in prior measurements of chlorophyll *a*, primary productivity at depth, and oxygen in a particularly well-studied region of the world ocean. Episodic phenomena continue to be undersampled in extant oceanographic databases, and the prospects for capturing them in traditional time-series mode are statistically humbling (43). More complete assessment of the influence of eddies on biogeochemical cycling will require models that fully resolve these processes. Existing models differ in this regard, some indicating little integrated impact (44) and others suggesting that eddies are the dominant mechanism of nutrient supply in the interior of the subtropical gyre (45). Improved estimates will require a number of revisions to prior models so that different responses in cyclones and mode-water eddies can be resolved. These include explicit representations of eddy/wind interactions and mechanistic links between mesoscale dynamics, species composition, and export.

References and Notes

1. New production is that fraction of total production supported by exogenous nutrients, as per Dugdale and Goering (46).

2. E. Shulenberg, J. L. Reid, *Deep-Sea Res.* **28A**, 901 (1981).
3. W. J. Jenkins, J. C. Goldman, *J. Mar. Res.* **43**, 465 (1985).
4. M. R. Lewis, W. G. Harrison, N. S. Oakley, D. Hebert, T. Platt, *Science* **234**, 870 (1986).
5. T. Platt, W. G. Harrison, *Nature* **318**, 55 (1985).
6. S. Emerson, S. Mecking, J. Abell, *Global Biogeochem. Cycles* **15**, 535 (2001).
7. D. G. Capone, J. P. Zehr, H. W. Pearl, B. Bergman, E. J. Carpenter, *Science* **276**, 1221 (1997).
8. D. Karl *et al.*, *Nature* **388**, 533 (1997).
9. N. Gruber, J. L. Sarmiento, *Global Biogeochem. Cycles* **11**, 235 (1997).
10. R. R. Hood, V. J. Coles, D. G. Capone, *J. Geophys. Res.* **109**, 10.1029/2002JC001753 (2004).
11. P. G. Falkowski, D. Ziemann, Z. Kolber, P. K. Bienfang, *Nature* **352**, 55 (1991).
12. D. J. McGillicuddy *et al.*, *Nature* **394**, 263 (1998).
13. A. Oschlies, V. C. Garçon, *Nature* **394**, 266 (1998).
14. A. Mahadevan, D. Archer, *J. Geophys. Res.* **105**, 1209 (2000).
15. M. Lévy, P. Klein, A.-M. Treguier, *J. Mar. Res.* **59**, 535 (2001).
16. J. D. Woods, in *Toward a Theory on Biological-Physical Interactions in the World Ocean*, B. J. Rothschild, Ed. (Reidel, Dordrecht, Netherlands, 1988), pp. 7–38.
17. R. G. Williams, M. J. Follows, in *Ocean Biogeochemistry: The Role of the Ocean Carbon Cycle in Global Change*, M. J. R. Fasham, Ed. (Springer, Berlin, Germany, 2003), pp. 19–51.
18. J. T. Allen *et al.*, *Nature* **437**, 728 (2005).
19. I. Dadou, V. C. Garçon, V. Andersen, G. R. Flierl, C. S. Davis, *J. Mar. Res.* **54**, 311 (1996).
20. V. H. Strass, *Deep-Sea Res.* **39**, 75 (1992).
21. S. A. Spall, K. J. Richards, *Deep-Sea Res. I* **47**, 1261 (2000).
22. E. N. Sweeney, D. J. McGillicuddy, K. O. Buesseler, *Deep-Sea Res. II* **50**, 3017 (2003).
23. B. Mouriño Carbillido, D. J. McGillicuddy Jr., *Limnol. Oceanogr.* **51**, 2675 (2006).
24. R. R. Leben, G. H. Born, B. R. Engebret, *Mar. Geodesy* **25**, 3 (2002).
25. Materials and methods are available as supporting material on Science Online.
26. D. K. Steinberg *et al.*, *Deep-Sea Res. II* **48**, 1405 (2001).
27. A qualitatively similar feature was observed at the BATS site in April 2001 (BATS 150), during which time a cyclone of similar magnitude was present at the time-series site.
28. We view this estimate as a lower bound on the implied remineralization, because this calculation ignores dilution of the oxygen deficit by mixing with waters outside the eddy core.
29. C. S. Davis, F. T. Thwaites, S. M. Gallagher, Q. Hu, *Limnol. Oceanogr. Methods* **3**, 59 (2005).
30. The small-scale (on the order of 10 km) fluorescence patchiness observed in the Video Plankton Recorder survey (Fig. 3A) is reminiscent of submesoscale frontal phenomena present in high-resolution numerical simulations (14, 15, 19, 21). Details of the relationship between, and interactions among, submesoscale and mesoscale processes remain a topic of active research. The key aspect of the observed fluorescence distribution as it pertains to diagnosis of the underlying mechanism is that the enhancement resides at the eddy center, not at the periphery.
31. Picophytoplankton concentrations determined by flow cytometry showed no significant difference in standing stocks of *Prochlorococcus* spp. or *Synechococcus* spp. between A4 and C1, although their relative contribution to total chlorophyll *a* decreased significantly in A4 because of the large diatom bloom (Fig. 2B).
32. J. D. McNeil *et al.*, *J. Geophys. Res.* **104**, 15537 (1999).
33. Ironically, the basin-scale pattern of low biomass and productivity of the subtropical North Atlantic has been attributed to the presence of mode waters (47), yet our results illustrate how mesoscale lenses of this water can create the most intense plankton blooms ever observed in the region.

34. Depth-integrated bacterioplankton biomass and production were not significantly different from the long-term mean at the BATS site. However, as compared to C1, volumetric bacterioplankton biomass and production in A4 were significantly enhanced within the deep chlorophyll a maximum, where diatoms dominated.
35. J. C. Goldman, D. J. McGillicuddy Jr., *Limnol. Oceanogr.* **48**, 1176 (2003).
36. Spectroradiometric observations of photosynthetically available radiation (PAR) in eddy A4 indicated that the depth of 1% of the surface value (a proxy for euphotic zone depth) had a mean of 96 m (SD = 9 m, $n = 37$ observations), which is nearly identical to that reported at the BATS site (48). Findings in C1 were similar, with a mean 1% PAR depth of 97 m (SD = 12 m, $n = 49$ observations).
37. S. Levitus, *NOAA Professional Paper No. 13* (U.S. Government Printing Office, Washington, DC, 1982).
38. Altimetric data point toward the northern source region for the 1-year period during which the eddy could be tracked (Fig. 1B). However, initial analysis of radioisotope measurements offers conflicting evidence: Radiocarbon data suggest a northern source, whereas tritium data suggest a southern source.
39. Nitrate-to-silicate ratios were similar in cyclone C1 and mode-water eddy A4. Concentrations in the upper euphotic zone were consistent with nitrogen limitation, because excess silicate (~ 1 to $2 \mu\text{mol kg}^{-3}$) was present in waters in which nitrate was depleted ($<0.1 \mu\text{mol kg}^{-3}$). All of the eddies we studied exhibited a similar tendency for the pycnocline to reside deeper than the nitracline, leading to supra-Redfield nitrate:phosphate ratios just below the euphotic zone. This enigmatic aspect is characteristic of the region (49, 50). Nevertheless, we could find no systematic differences in nitrate-to-phosphate ratios between cyclones and mode-water eddies.
40. A. P. Martin, K. J. Richards, *Deep-Sea Res. II* **48**, 757 (2001).
41. The Martin and Richards model (40) predicts the vertical velocity at the base of the layer through which wind stress can be transmitted directly through waves and turbulence (the Ekman layer). Quasigeostrophic theory and models demonstrate that this vertical motion penetrates well into the inviscid interior, diminishing with depth (51). We ran a primitive equation model simulation of eddy A4, which indicated that the vertical velocity at the depth of the high-chlorophyll layer was $\sim 90\%$ of the Ekman upwelling velocity. The physical manifestation of this effect is a tendency for upward displacement of the seasonal pycnocline at the eddy center, enhancing the mode-water eddy structure (Fig. 1A).
42. This model also predicts upwelling in the interior of regular anticyclones. An analogous phenomenon has been hypothesized to upwell depressed density surfaces in the interiors of warm-core Gulf Stream rings (51), a process that would tend to enhance biological activity associated with their frictional decay (52).
43. D. M. Karl, E. A. Laws, P. Morris, P. J. I. B. Williams, S. Emerson, *Nature* **426**, 32 (2003).
44. A. Oschlies, *Global Biogeochem. Cycles* **16**, 1106 (2002).
45. D. J. McGillicuddy, L. A. Anderson, S. C. Doney, M. E. Maltrud, *Global Biogeochem. Cycles* **17**, 1035 (2003).
46. R. C. Dugdale, J. J. Goering, *Limnol. Oceanogr.* **12**, 196 (1967).
47. J. B. Palter, M. S. Lozier, R. T. Barber, *Nature* **437**, 687 (2005).
48. D. A. Siegel *et al.*, *Deep-Sea Res. II* **48**, 1865 (2001).
49. A. F. Michaels *et al.*, *Deep-Sea Res.* **41**, 1013 (1994).
50. J. Wu, W. Sunda, E. A. Boyle, D. M. Karl, *Science* **289**, 759 (2000).
51. W. K. Dewar, G. R. Flierl, *J. Phys. Oceanogr.* **17**, 1653 (1987).
52. P. J. S. Franks, J. S. Wroblewski, G. R. Flierl, *J. Geophys. Res.* **91**, 7603 (1986).
53. R. M. Letelier *et al.*, *Limnol. Oceanogr.* **38**, 1420 (1993).
54. We thank the officers and crews of the *R/V Oceanus* and *R/V Weatherbird II* for their outstanding support during our seagoing operations. R. Leben provided near-real-time altimetric data that were crucial for our adaptive sampling effort. Nutrient samples were processed by the Nutrient Analytical Facility (P. Henderson) at the Woods Hole Oceanographic Institution. Numerical simulations were performed at the National Center for Atmospheric Research's Scientific Computing Division. We thank O. Kosnyreva for expert data analysis and visualization and S. Stasiowski for administrative support. We gratefully acknowledge the efforts of all participants in the EDDIES project, which included a number of BATS technicians. For more information, see http://science.whoi.edu/users/olga/eddies/EDDIES_Project.html. The EDDIES project was funded by NSF's Chemical, Biological, and Physical Oceanography Programs. Additional support for remote sensing aspects (including altimetry and QuikSCAT wind analyses) and high-performance liquid chromatography pigment assays (C. Trees, Center for Hydro-Optics and Remote Sensing) was provided by NASA.

Supporting Online Material

www.sciencemag.org/cgi/content/full/316/5827/1021/DC1

Materials and Methods

Fig. S1

Tables S1 to S3

References

12 October 2006; accepted 13 February 2007

10.1126/science.1136256

Stress Control of Deep Rift Intrusion at Mauna Loa Volcano, Hawaii

Falk Amelung,^{1,*} Sang-Ho Yun,² Thomas R. Walter,^{1,†} Paul Segall,² Sang-Wan Kim¹

Mauna Loa volcano, Hawaii, deforms by a combination of shallow dike intrusions in the rift zones and earthquakes along the base of the volcano, but it is not known how the spreading is accommodated in the lower part of the volcanic edifice. We present evidence from interferometric synthetic aperture radar data for secular inflation of a dike-like magma body at intermediate depth in the southwest rift zone during 2002 to 2005. Magma accumulation occurred in a section of the rift zone that was unclamped by previous dikes and earthquakes, suggesting that stress transfer plays an important role in controlling subsurface magma accumulation.

Modern volcano-monitoring techniques can detect precursory seismic unrest months to days before an eruption, but information about possible eruption locations is generally not available. Such information is important for hazard assessment and for timely warning of the population for large and populated basaltic shield volcanoes such as Mauna Loa volcano in Hawaii. Forecasting the eruption location requires a better understanding of subsurface magma

migration. Here we show that the 2002 to 2005 magma intrusion at Mauna Loa volcano inferred from space-geodetic data is consistent with changes in the stress due to the previous tectonic and magmatic events. This suggests that the stress field within the volcanic edifice is a dominant effect in controlling magma accumulation. Space-geodetic measurements can be used to infer changes to the stress field in the interior and contribute to better forecasts of the response of a volcano to the arrival of new magma from below.

Mauna Loa volcano is the largest and one of the most active volcanoes on Earth. It has produced more than 4 km^3 of lava during the past 150 years (1). Most historic eruptions involved the propagation of an eruptive fissure from the summit downrift into the northeast rift zone (NERZ) or into the southwest rift zone (SWRZ) (Fig. 1A). About

30 to 40% of the volcano's subaerial surface has been covered by new lava during the past 1000 years. Thus, a large portion of the island is threatened by lava flows, and it is very important to better estimate where possible eruptions could occur. The last major eruptions occurred in 1950 from the SWRZ and in 1984 from the NERZ. At Mauna Loa, repeated dike intrusions into the rift zone result in seaward motion of the volcano flanks, most of which is believed to be accommodated in form of seismic or aseismic displacement along a decollement fault on the paleo-seafloor at the base of the volcanic edifice at 12- to 14-km depth below the summit. The 1868 magnitude (M) 8 Pahala (2) and the 1951 M 6.9 Kona earthquakes (3) likely ruptured the decollement.

Inflation at Mauna Loa volcano started in May 2002 at the same time when Kilauea volcano increased its rate of lava production (4). Subcrustal seismicity increased in 2004 (Fig. 1A). We used interferometric synthetic aperture radar (InSAR) acquired by the Canadian Radarsat-1 satellite between 2001 and early 2006 to obtain a detailed image of the ground deformation associated with the volcanic inflation. InSAR measures the change in distance between the ground and the satellite in radar line-of-sight (LOS) direction. We used imagery with different incidence angles of the radar beam and an average of five to nine interferograms each spanning 3 to 4 years for each viewing geometry (table S1) to obtain averaged LOS velocities for the period May 2002 to end 2005 (5). Averaging interferograms increases the signal-to-noise

¹Rosenstiel School of Marine and Atmospheric Sciences, University of Miami, 4600 Rickenbacker Causeway, Miami, FL 33149, USA. ²Department of Geophysics, Stanford University, Stanford, CA 94305, USA.

*To whom correspondence should be addressed. E-mail: famelung@rsmas.miami.edu

†Present address: GeoForschungsZentrum Potsdam Section 2.1, Telegrafenberg, 14473 Potsdam, Germany.